



Quantifying residential PV feed-in power in low voltage grids based on satellite-derived irradiance data with application to power flow calculations



Holger Ruf^{a,c,*}, Marion Schroedter-Homscheidt^b, Gerd Heilscher^a, Hans Georg Beyer^c

^aUlm University of Applied Sciences, Institute of Energy and Drive Technologies, Eberhard-Finckh-Strasse 11, 89075 Ulm, Germany

^bGerman Aerospace Center, German Remote Sensing Data Center, Oberpfaffenhofen, 82234 Wessling, Germany

^cUniversity of Agder, Department of Engineering Science, Jon Lilletunsvai 9, Grimstad, Norway

ARTICLE INFO

Article history:

Received 10 December 2015

Received in revised form 31 May 2016

Accepted 1 June 2016

Keywords:

Heliosat method

Distribution network

Residential photovoltaic

Low voltage grid

CAMS radiation service

Earth observation

ABSTRACT

A scheme using satellite-derived irradiance measurements to model the feed-in power of residential photovoltaic (PV) systems in a low voltage distribution grid is described. It is validated against smart meter measurements from a test site with 12 residential PV systems in the city of Ulm, Germany, during May 2013 to December 2014. The PV feed-in power is simulated in a 15-min time resolution based on irradiance data derived from Meteosat Second Generation satellite images by the physically based retrieval scheme Heliosat-4. The PV simulation is based on the nominal power and location of the PV systems as provided by the distribution system operator. Orientation angles are taken from high resolution aerial laser-scan data. The overall average mean error of PV feed-in power is 4.6% and the average root-mean-squared error is 12.3% for the individual systems. Relative values are given with respect to the total installed power of 152.3 kWp. Sensitivity studies discuss the need for knowing the exact orientation angles of each individual PV system or the usefulness of a single ground-based measurement as alternative to satellite observations. As an application of the scheme, the modelling of the effect of the power flow from the residential PV on the load flow of the low voltage distribution grid transformer is described and illustrates the advantage of the discussed approach for distribution system operators.

© 2016 The Authors. Published by Elsevier Ltd. This is an open access article under the CC BY license (<http://creativecommons.org/licenses/by/4.0/>).

1. Introduction

In Germany, the majority of photovoltaic (PV) systems is installed in residential areas and connected to the low voltage distribution electricity grids. A major increase in the number of PV systems has been observed in recent years, causing new challenges for the electricity grid management (DGS, 2015).

Grid stability and power quality at the low voltage level is guaranteed by the distribution system operators (DSO). Nowadays the interconnections between the high and medium voltage grid are monitored widely in real time. Also, remote controllable devices exist to actuate the grid. On the other hand, at the interconnections between the medium and the low voltage grid only current meters with slave pointers are used. These only show the real-time readings but do not store or transmit the data for further analysis. Additionally, they allow monitoring the maximum apparent power at a

transformer station which occurred since the last readout. Typically, the readout is only done manually once a year. In order to improve the monitoring capabilities a significant addition of controllable devices in the low voltage grid is currently foreseen (e.g. Agricola et al., 2014).

DSOs have to plan, operate, and maintain the grid to avoid voltage band violations and overloading of grid assets (EnWG, 2013). In doing so, their objective is to avoid unnecessary investments in *brute force* grid reinforcement. This may occur due to missing knowledge on the PV power contribution in different grid sections. There is a need for a cadaster of existing PV systems. DSOs require accurate information on distributed energy resources in the electric grid in order to fulfill their responsibility for grid operations (EnWG, 2013; NAV, 2006; TAB, 2009). On the other hand, solar surface irradiance time series over e.g. the last ten years and in 15-min temporal resolution are required to realistically simulate the recent PV feed-in power under the assumption of increasing solar shares. Having in mind that any expansion of the grid infrastructure will last over decades, the need for reliable planning data and simulation tools is obvious. Both, the potential maximum

* Corresponding author at: Ulm University of Applied Sciences, Institute of Energy and Drive Technologies, Eberhard-Finckh-Strasse 11, 89075 Ulm, Germany.
E-mail address: ruf@hs-ulm.de (H. Ruf).

and the current feed-in active power of the grid-connected PV systems at any point in time in all their grid sections and at the transformer station level are required.

There is a gap between available methodologies for simulating and monitoring the individual PV system and the sum of PV feed-in power at the transformer station at low voltage level. Fig. 1 gives a schematic view of the factors affecting the load flow at the transformer. Besides the load in the low voltage grid segment, the variable PV generation needs to be simulated as a sum of the individual PV systems. The latter is a function of the respective PV system type and size as well as the irradiance on the module plane at each PV system.

The influence of distributed PV systems on the load flow in the distribution grid on both low and medium voltage levels has been described e.g. in Pardatscher et al. (2011). They derived the load flow for a total of 910 PV systems in a 12 km × 12 km area in southern Germany. However, the study was only for an assumed clear-sky day and another single day with large fluctuations as extreme cases. The day-to-day behavior remains an open question.

For realistic modelling of the real PV feed-in power, accurate measurements of irradiance conditions have to be available. Up to now, ground measured irradiances are used typically for the simulation of individual residential PV systems. Ueda et al. (2009) investigates the performance of 553 roof-mounted residential PV systems with various orientations by taking into account the local irradiance measured by a single pyranometer.

Such ground measurements are point measurements only and do not fully represent the natural spatial and temporal variability of a distributed PV fleet (Lave et al., 2013). In contrast, satellite-based irradiances provide the spatially distributed information, but with restrictions in the available spatial and temporal resolution. Typically, satellites have several km-sized pixels and 5 to 15-min temporal resolution. On the other hand, time series can be provided for more than 10 years. Satellite irradiance data may therefore fulfill the DSOs' needs for historical and spatially resolved information at 15-min time steps. This paper assesses the suitability of this approach.

PV simulation studies have been making use of satellite-based data to some extent. Leloux et al. (2012a,b) assessed the performance of more than 7000 residential PV systems in France and Belgium but using monthly irradiation only. Also they did not relate it to the load flow. The performance simulation and interaction of a PV fleet distributed over an area of 11 km × 15 km with 15-min irradiances derived from satellites is reported in Grossi et al. (2014). They assumed only a singular orientation for all systems. A similar approach was taken by Hoff and Perez (2012) for the determination of the variability of PV feed-in power

on the macro scale area with a range from 10 km to 300 km. Bucher et al. (2012) used 15-min satellite data to derive statistical values for a given location to generate synthetic high resolution PV feed-in power profiles by Monte-Carlo simulations. These synthetic PV feed-in power profiles are used for the calculation of the hosting capacity for distributed PV systems in grids, taking into account various load profiles. However, only statistical reference grids are used instead of a real electric grid topology and a comparison against smart meter measurements is not provided. Rikos et al. (2008) have shown the suitability of using satellite-based irradiances to simulate the voltage at a substation for selected test cases in the island grid of Kythnos, Greece. Sky imagers are an alternative to satellite data and provide even higher spatial and temporal resolution, but sky imagers are only deployed in a few places and over short periods of time (Nguyen et al., 2016).

For the management of large scale transmission systems with a significant amount of PV penetration in Europe (Kühnert et al., 2014) and the U.S. (Renné, 2014), the use of satellite derived irradiation information is state-of-the-art. The information gap concerning the lack of monitoring individual PV systems with their orientation and system data, is virtually closed by using a lumped PV model, representing the average response of the PV fleet (Beyer et al., 2004). This requires that the number of PV systems covered is sufficiently large in order to average out the specific peculiarities of individual systems. Within this type of studies, details of planning and operation at the low voltage level are not handled.

A part of the information gap, especially the PV system orientation, can be closed with 3D data from geographical information systems. The combination of using both digital elevation models based on airborne laserscan data and solar irradiance data is state-of-the-art for the calculation of the received annual solar energy on tilted module planes. Fath et al. (2015) apply this approach by using irradiance data from the Meteornorm database (Meteotest, 2015). Jakubiec and Reinhart (2013) take 15-min irradiance data from a meteorological station nearby. Verso et al. (2015) use satellite-based time series of irradiances. However, all these studies focus on the theoretical solar potential on roofs in urban sites and not on the feed-in power of existing PV systems.

Normally, the DSO knows only the location of the connection point and the nominal power of the PV system, but not the individual orientation angles or the shadowing for each system due to obstacles in the neighborhood. Therefore, an objective of this study is to work with these imperfect limited data and not with all information available from a well-known test site as e.g. module and inverter types or PV mounting systems. Nevertheless, in order to quantify this information gap, the orientation angles of the

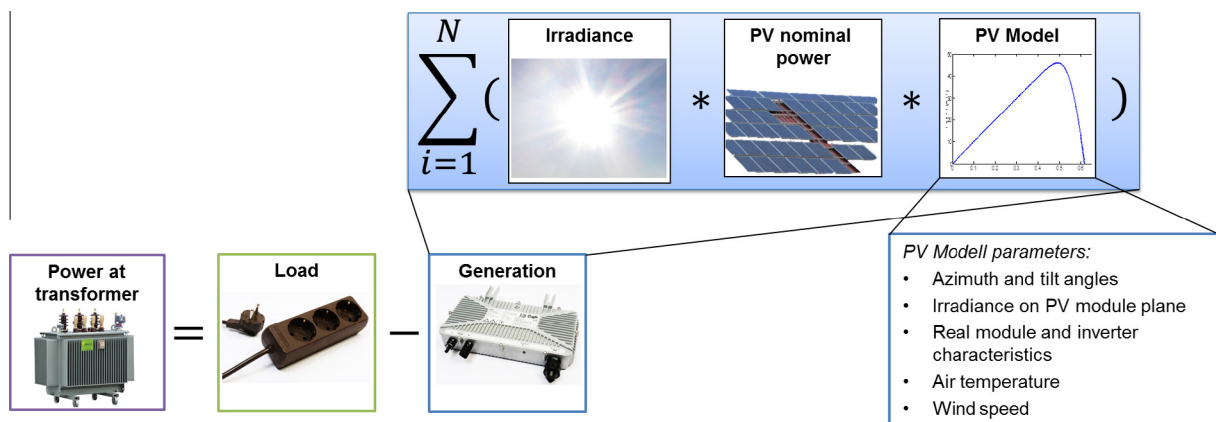


Fig. 1. Schematic study setup for simulation of the feed-in power of residential PV systems.

investigated PV systems are also determined in very high accuracy from a solar potential analysis based on airborne laser-scan data.

The calculated 15-min averages of the feed-in active power of the individual PV system are validated against the 15-min averages of the active power measurement from the feed-in smart meters of 12 PV systems.

DSOs are also interested in the question whether the model can reflect the probability of occurrence of extremes in the time series. Such extremes can be defined as the case that a specific PV system reaches a defined feed-in power threshold as e.g. 70% or 100% of the nominal power. The 70% threshold is chosen according to current legal requirements in Germany (EEG, 2014). This law requires for PV systems up to 30 kWp nominal power to either generally reduce their maximum feed-in power to this threshold or have to install a feed-in management system which is remotely controllable by the responsible DSO. Below, we analyse whether the occurrence of feed-in power larger than 70% of the PV system's nominal power can be derived based on satellite irradiance data in a sufficient accuracy.

The paper is organized as follows: Section 2 describes the datasets used for the simulation and validation. The PV simulation model is introduced in Section 3. In Section 4 the simulation is validated against measurements. Section 5 validates the application for threshold detection. An example for the application of the simulated PV feed-in power data in a grid and transformer simulation is given in Section 6. Finally, conclusions and future directions are given in Section 7.

2. Data sources

2.1. Test site

The test site is a suburban residential area in the city of Ulm, southern Germany. It covers the area of 470 m × 615 m and is supplied via a 630 kVA medium-to-low voltage transformer (Fig. 2). 133 houses are attached via eight feeder lines.

At the test site, there are 21 roof-mounted residential PV systems (named PV1 to PV21) installed with an overall nominal power $P_{nom} = 233$ kWp and ranging from 2.2 kWp to 47.84 kWp each. The average nominal power per roof is 11.07 kWp which is close to the average value of residential PV system nominal power as reported for southern Germany (Wirth et al., 2011). The PV systems are distributed over the whole test site. Smart meters are installed at 12 PV systems providing 15-min average feed-in active power values since May 2013. Table 1 summarizes nominal power, orientation and inclination of the monitored PV systems. The total monitored nominal power of the 12 PV systems is 152.3 kWp. Usually, the DSO only knows the location and the nominal power of the PV systems. In our study, the tilt and azimuth angles are extracted from laser-scan data (Ruf et al., 2015). The error of these angles is less than 10°. An azimuth angle of 180° represents south orientation.

The PV feed-in power measurements are based on Landis & Gyr ZMD310 smart meters. This type is rated as class B according to DIN EN 50470-3 (2007) and by law the allowed calibration error limit ranges from 2% to 3%. A control of their accuracy at the meter test facility of the local DSO showed errors for the power measurement below 0.5% (Katzmaier, 2015). The calculation of the PV power feed-in starts 15th May 2013 and ends 14th December 2014 because of the availability of the smart meters provided by the DSO measurement campaign.

2.2. Meteorological data

Irradiance data are taken from the Copernicus Atmosphere Monitoring Service (CAMS) Radiation Service (Qu et al., in press). They are derived from Meteosat Second Generation (MSG) satellite images with a 15-min time resolution based on the Heliosat-4 approach (Oumbe et al., 2014; Lefèvre et al., 2013). MSG satellite images have a pixel resolution of 3 km² at nadir of the field of view. The resolution at the test site is approximately 5 × 3 km².



Fig. 2. Aerial image of the test site. The border is marked with a blue polygon. The investigated PV systems with smart meters are marked in red. (For interpretation of the references to color in this figure legend, the reader is referred to the web version of this article.)

Table 1

Parameter list of monitored PV systems in the test site. Note: PV14 and PV15 have only one common smart meter (marked with *).

PV system	Azimuth angle [°]	Tilt angle [°]	P_{nom} [kWp]
PV1	90	25	47.8
PV2	180	46	13.0
PV8	153	46	9.6
PV10	180	42	4.8
PV13	153	45	6.5
PV14*	90	42	8.6
PV15*	180	36	2.9
PV16	153	33	7.8
PV17	206	35	17.0
PV18	206	33	10.6
PV19	153	35	7.4
PV20	180	47	8.2
PV21	243	42	8.1

Further meteorological data required for the simulation are air temperature and wind speed. These data are taken from the roof-mounted meteorological station operated by Ulm University of Applied Science (48.42°N, 10.00°E, height 550 m above sea level). The data were analyzed for missing data but no such data were found. Temperature is measured with a Thies 'hygro-thermo transmitter compact'. Wind speed and direction are measured with a Thies 'windsensor classic' which is a cup-anemometer in combination with wind direction sensors. The distance to the test site is 11 km. Both the location of the test site and ground measurement as well as the size of the satellite image pixels are shown in Fig. 3. The distance in the measurements leads to deviations due to local effects on the air temperature as urban heat islands or roof temperature as well as wind effects based on the orography and building

structures. Their influence is unknown, however according to Krauter et al. (2008) an error of 2% in air temperature leads to an error in the annual PV yield of 0.5% and 50% in wind speed at module to 1.5% in the annual PV yield, respectively. Furthermore, DSOs normally operate weather stations measuring air temperature, wind speed and illumination somewhere at their grid area, e.g. at the substations or at buildings. These stations often do not comply with the WMO requirements as e.g. being over a grass surface and shaded in a white colored weather shelter (WMO, 2008). Additionally, having ground-based GHI observations available is not state-of-the-art in daily DSO operations. Additionally, having ground-based GHI observations available is not state-of-the-art in daily DSO operations. The authors assume that the approach is realistic and justified according to the general data availability practice in DSO even if the risk of inaccuracy is existing.

The distance between the ground measurement of the temperature and the test site is accepted with respect to the required accuracy of temperature and wind speed in PV plant modelling. The 10-min averaged data from the university meteorological station are compared with data from the weather station operated by the German Weather Service. This station is located between the test site and the university weather station. The comparison of the air temperature results in a mean difference of 0.07% and a root-mean-squared deviation (RSMD) of 6.6%. The errors of the wind speed comparison are higher (mean difference 6.7%, RMSD 32.3%) but still negligible for the PV systems following Krauter et al. (2008). Thus, the data from weather station at the university have a sufficient quality and the spatial variation of the temperature is small.

Besides using satellite data, global horizontal irradiance (GHI) is also measured at the Ulm University site with a calibrated



Fig. 3. Overview of the test site location (green-filled polygon), location of the ground-measured irradiance (blue star) and the pixel-size of the MSG satellite (pixel corners are marked with red crosses). Grey lines indicates the different districts of ULM. (For interpretation of the references to color in this figure legend, the reader is referred to the web version of this article.)

pyranometer (First class according to WMO (ISO 9060, 1990)) manufactured by Theodor Friedrichs GmbH & Co. The 15-min average GHI ground observations are available from 1st January 2012 to 31st December 2014 with a lack of data in June 2013 due to a data logger failure.

3. Photovoltaic system model

The calculation of the feed-in power for each PV system is performed with the PVLib provided by the Photovoltaic Performance Modelling Collaborative (PVMC; Stein, 2012). This library offers the flexible input of detailed meteorological data in the electrical system modelling of PV systems.

For irradiance data, input parameters are global (GHI), diffuse (DHI) and direct (BHI) irradiances on the horizontal planes as e.g. delivered by CAMS Radiation Service. Irradiances in the module plane are calculated using the approach of Reindl et al. (1990a,b) for the diffuse fraction.

DSOs typically consider the orientation of PV systems for grid planning or operations by using the same theoretical optimum orientation for each system because they do not know installation details. However, often they resort only to a coincidence factor of the PV feed-in power (Pardatscher et al., 2011). Therefore, we also conduct a PV simulation model using a single orientation for all systems. The consideration of multiple orientations would significantly increase the time and effort in identifying and modelling PV systems. This can be done manually for a small number of PV systems like in the test site but not in a larger grid area as Ulm with more than 4000 PV systems.

Additionally, PV systems with different azimuth angles are rather seldom. An optical inspection based on aerial images of 442 PV systems in Ulm shows that 39 PV systems (8.8%) have two different azimuth angles and only 15 systems (3.4%) have three or more orientations. Therefore, only a single orientation is applied for the modelling. Actually, PV1 in our study is a PV system with panels at different orientations. This will probably result in larger errors for this system, but this disconnect between reality and model parameters mirrors the approach that DSOs would take.

The treatment of the ground reflected part follows Loutzenhiser et al. (2007) with an albedo value of 0.2 (Fath et al., 2015). The albedo is kept constant for each system and each time step. Effects like snow cover or seasonal changes in the surrounding vegetation are neglected.

For the system modelling a poly-crystalline PV module type is selected from the PVLib library. This is justified by the fact that this technology is mostly used in Germany (Glunz et al., 2012). The module technology information refers to the Sandia PV Array Performance Model (SAPM) and Sandia Performance Model for Grid-Connected Photovoltaic Inverters coefficients (King et al., 2004, 2007). The chosen PV module type is 'Yingli Solar YL230-29b' together with a 'Blueplanet 6400xi supreme' inverter produced by Kaco New Energy GmbH as the inverter type.

The PV system simulation uses global irradiance on the tilted plane (GTI), air temperature and wind speed to calculate the cell temperature using the approach of King et al. (2004).

The real PV module string configurations of the single PV systems are unknown in this study. But again, this reflects the typical DSOs state of knowledge and is therefore accepted. A typical string configuration for a residential system is assumed (Albrecht and Schröder, 2013). This configuration leads to a typical PV system of 28 PV modules from the type as mentioned before, which are divided into two strings with 14 modules each. These two strings are connected to a single PV inverter. The inverter AC rating to PV DC rating sizing ratio is one. The calculated output power time series of this reference PV system is normalized to the PV generator

nominal power under standard test conditions and scaled up to the nominal power of the installed PV modules at the test site. Each PV system is treated with its individual orientation angles but with the same assumption on its internal string structure. In the simulation it is assumed that losses due to the system set-up (e.g. wiring losses) or due to the maximum power point tracker of the inverter are negligible. Typically, residential PV systems are designed such that the cable losses are below 1% of the rated power (Albrecht and Schröder, 2013). The efficiency of maximum power point tracker systems and DC/AC converters ranges from 96% to 99% (Bendib et al., 2015). Both losses are within the tolerance of the PV module rating and not determinable without additional system-specific information. Finally, the feed-in power is calculated for each single PV system in a temporal resolution of 15 min.

4. Validation

4.1. Validation of satellite-based irradiance data

The deviation of the Heliosat-4 approach compared to ground measurements of the GHI is analyzed. Based on the benchmarking guidelines developed during the MESoR project (Beyer et al., 2009), the root-mean-squared error (RMSE), mean error (ME) and correlation coefficient (CC) are defined as in Eqs. (1)–(3):

$$ME = \frac{1}{N} \sum_{i=1}^N x_s(i) - x_m(i), \quad (1)$$

$$RMSE = \sqrt{\frac{1}{N} \sum_{i=1}^N (x_s(i) - x_m(i))^2}, \quad (2)$$

$$CC = \frac{\sum_{i=1}^N (x_s(i) - \bar{x}_s) \cdot (x_m(i) - \bar{x}_m)}{\sqrt{\sum_{i=1}^N (x_s(i) - \bar{x}_s)^2 \cdot \sum_{i=1}^N (x_m(i) - \bar{x}_m)^2}}, \quad (3)$$

where N is the total number of measurement data points, $x_s(i)$ is simulated data at time i and $x_m(i)$ is measured data at time i . The temporal resolution of CAMS Radiation Service is 15 min. Each value is the irradiation as sum of 1-min values of the previous 15 min. The ground measurements are averaged in the same manner from 1-min irradiation measurements. The relative values of ME and RMSE are rated to the mean values of the daytime measurements and denoted as rME and rRMSE. The clear-sky index kC is defined as the ratio of the GHI to GHI under cloud-free conditions, both taken from CAMS Radiation Service.

Other studies often consider only irradiance data with sun elevation angles above 15°. We follow this approach. The analysis (Fig. 4) results in a ME of 21.9 W/m² (rME 6.1%), an RMSE of 115.9 W/m² (rRMSE 32.4%) and a CC of 0.90. CAMS Radiation Service shows a significant scatter and a general overestimation probably due to clouds over the ground measurement locations, which are in a sub-pixel scale related to the satellite pixel resolution. In such cases CAMS Radiation Service detects an almost clear sky with a satellite-based kC around or just below one while the ground measurement is smaller due to a local cloud.

The linear regression for CAMS Radiation Service (GHI_M) versus pyranometer (GHI_P) data results in $GHI_M = 0.83 * GHI_P + 81.33$ W/m². The overall overestimation of CAMS Radiation Service during low irradiance conditions and an underestimation in high irradiance cases is visible.

The validation of GHI in this study is performed for a single point only and does not give a general answer about the accuracy of the Heliosat-4 data from CAMS Radiation Service. However, the results are in line with other published results (Qu et al., in press). It can therefore be assumed that there are no local effects in the area of Ulm blocking the usage of the satellite data.

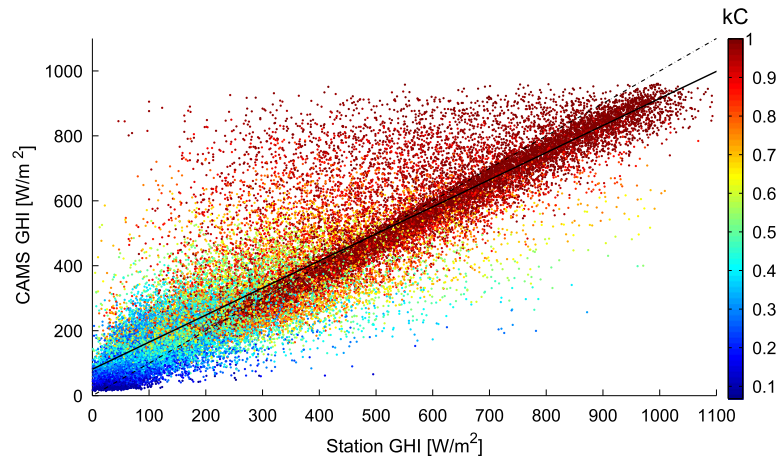


Fig. 4. Comparison between ground measured and satellite measured 15-min GHI averages. The black solid line indicates the linear regression and the black dash-dotted line indicates the main diagonal. The clear-sky index kC is color-coded. (For interpretation of the references to color in this figure legend, the reader is referred to the web version of this article.)

It is assumed that satellite pixels are helpful to describe the natural variability inside a distribution grid of the city-size as e.g. in Ulm. Nevertheless, due to missing distributed ground measurements, the accuracy in representing the spatial and temporal variability of GHI by the various satellite pixels cannot be assessed directly. On the other hand, there is a sub-scale variability inside the pixel which can also not be assessed by comparing to a single ground measurement location. However, this effect will be considered implicitly by comparing against feed-in power of each PV system individually.

4.2. Validation of satellite-based simulations of PV feed-in power

This section describes the validation of satellite-based PV feed-in power versus the smart meter measurements obtained at each PV system. Besides the individual values at each PV system also the averages and the summation on the transformer level (PV fleet) are investigated in order to have a detailed view. All statistical results including the ME, RMSE and CC of the simulated PV feed-in power are listed in Table 2. Fig. 5 shows the 15-min averages of both simulation and measurements for each PV system. All systems show positive biases probably due to the positive GHI biases in CAMS Radiation Service, but PV1 obviously differs from the other systems.

Table 2
Quality measures of the 15 min averaged PV feed-in power simulations based on Heliosat-4 derived irradiances against smart meter measurements for the 12 systems analyzed in the period from 15th May 2013 to 14th December 2014.

PV system	ME [kW]	RMSE [kW]	CC	nME [kW/kWp]	nRMSE [kW/kWp]
PV1	2.63	7.67	0.75	0.05	0.16
PV2	0.39	1.67	0.89	0.03	0.13
PV8	0.44	1.22	0.89	0.05	0.13
PV10	0.29	0.65	0.89	0.06	0.14
PV13	0.24	0.81	0.89	0.04	0.12
PV14 + 15	0.39	1.24	0.89	0.04	0.14
PV16	0.37	1.01	0.89	0.05	0.13
PV17	0.89	2.27	0.88	0.05	0.13
PV18	0.37	1.4	0.88	0.04	0.13
PV19	0.21	0.93	0.89	0.03	0.13
PV20	0.5	1.14	0.88	0.06	0.14
PV21	0.41	1.06	0.88	0.05	0.13
PV fleet	7.12	18.73	0.87	0.05	0.13
Mean w/o PV1	0.41	1.22	0.89	0.04	0.13

Typically, the Heliosat algorithm is only valid with sun elevation angles above 15° (e.g. Zarzalejo et al., 2009). However, PV systems start operating as soon as GHI reaches a PV system specific minimum value. This may occur at sun elevation angles below 15°. Therefore, the validation of the PV feed-in power is performed for all sun elevation angles above 0° while all validation results in Section 4.1 excluded sun elevation angles below 15° to ensure comparability to other studies.

PV1 shows an extended overestimation because of its multiple orientations with parts of the PV modules being oriented to the East and others to the West. The aerial image confirms a majority of PV modules on the western roof. As the simulation model uses a single tilt and azimuth angle for each PV system, a low correlation with real measured values is caused and expected. As mentioned before, such systems are rare. Therefore, it is accepted that the simulation is not working sufficiently in this case and PV1 is excluded from the mean results below. Nevertheless, the system is not completely excluded to (a) show the impact and (b) to allow also the assessment of the fleet of all PV systems in the real test site.

The measured data of PV8 shows a defined upper limit of the feed-in power at 70% of the rated power. This may be a result of the German Renewable Energy Law (EEG, 2014) calling for a limitation of the feed-in power to a fraction of the nominal power if no device for external control is installed. This limitation was not considered in the satellite model. The combined PV system (PV14 + PV15) is the only system that reaches a feed-in power of more than the nominal power.

The ME ranges from 0.21 kW to 0.89 kW with an additional outlier of 2.63 kW at PV1 due to its two-sided orientation. Overall, this results in an averaged ME of 0.59 kW and of 0.41 kW if PV1 is excluded as outlier. Considering the average PV system size of 12.67 kWp this is a rME = 4.6% and 3.6%, respectively. The RMSE ranges from 0.65 kW to 2.27 kW with the PV1-based outlier of 7.67 kW. The overall average for all PV systems is 1.76 kW (rRMSE = 13.9%) and 1.22 kW (rRMSE = 9.6%) if PV1 is excluded. The CC is around 0.88 with the outlier of 0.75 for PV1. The accumulated PV feed-in power at transformer level results in a ME of 7.12 kW (rME = 4.6% related to the total monitored PV system size of 152 kWp) and an RMSE of 18.73 kW (rRMSE = 12.3%), while the CC is 0.87.

Furthermore, the ME and RMSE are normalized to the nominal power of each PV system. The normalized ME ranges from 0.03 kW/kWp to 0.06 kW/kWp with a mean of 0.05 kW/kWp. The normalized RMSE ranges from 0.12 kW/kWp to 0.16 kW/kWp with

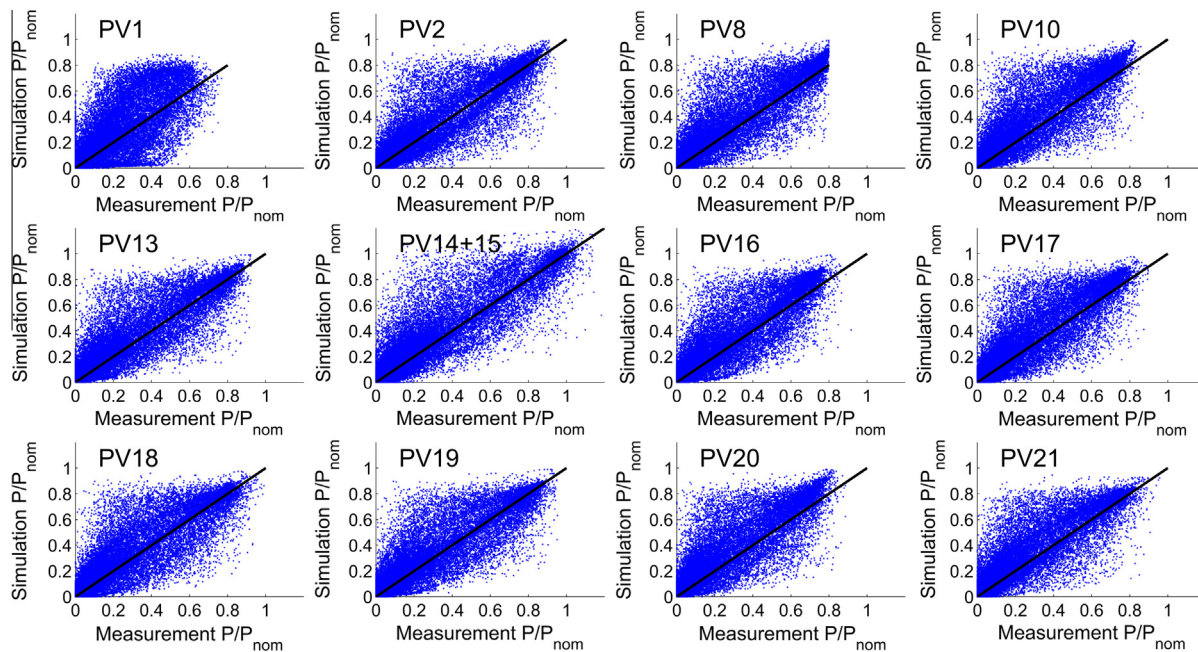


Fig. 5. Comparison between measured normalized PV feed-in power and simulated feed-in power with CAMS Radiation Service irradiance data for all 12 PV systems.

a mean of 0.14 kW/kWp. The normalized values show that the errors are independent of the PV system size and generally satisfying for residential PV simulations and for grid planning issues. A positive ME is beneficial over a negative ME as the resulting over-estimation of PV production provides a safety margin for grid operations. A negative ME would reduce the reserve provided by the DSO (Meier, 2014) and would be seen as an additional risk.

A case study in US (Stein et al., 2010) finds a normalized ME of 0.03 kW/kWp and a normalized RMSE of 0.10 kW/kWp for the calculation of the PV DC power using hourly satellite irradiance data. The similar value of the normalized ME is appreciable. The satellite-based GHI data in the US-study are bias-free and the normalized ME only depends on the PV model. The normalized ME in our work consists of the bias of CAMS Radiation Service as well as a bias of the PV model. The lower RMSE results compared to our work may be due to the lower time resolution and the higher stock of PV system information.

4.3. Sensitivity to module type

Changing the module type of the reference PV system in the PV simulation model results in minor differences. If a mono-crystalline-silicon module (type: SunPower SPR-230-WHT) is used instead of the poly-crystalline-silicon module, the overall ME is slightly reduced by 0.06 kW because of the outlier of PV1. The difference of the other PV systems is below 0.01 kW. The RMSE increases in the range of 0.0 kW to 0.05 kW with an outlier of 0.11 kW for PV1. The overall RMSE is 0.26 kW higher compared to the RMSE using the poly-crystalline-silicon module in the PV model. These results are a deviation of less than 2% and below the typical rating tolerance of PV modules.

As a second variation a thin-film PV module (type: First Solar FS-275) is assumed for the modelled reference PV system. The overall ME is reduced by 0.82 kW. The outlier of PV1 is 0.31 kW while the reduction of the other PV systems ranges from 0.02 kW to 0.07 kW. The RMSE increases in the range of 0.0 kW to 0.05 kW with an outlier of 0.14 kW for PV1. The overall RMSE is 0.21 kW higher compared to the RMSE using the poly-crystalline-silicon module in the PV model. In both variations the difference

of CC is below 0.3% related to the CC using the poly-crystalline-silicon module in the PV model. If thin film modules are assumed, the ME is reduced by approximately 15% while the RMSE is increased by around 1%. Note that thin film modules are seldom used in Germany.

4.4. Sensitivity to orientation

Generally, for Ulm a 30° tilt angle oriented to the South is considered as optimal in PV system planning. Using this angle orientation instead of the actual one for the PV systems, both ME and RMSE increase. Fig. 6 shows the results for each PV system from this variation (rectangles) and the original results from Section 4.2 (crosses).

The ME ranges from 0.27 kW to 0.92 kW with an additional outlier of 2.63 kW at PV1. Overall, this results in a mean of 0.87 kW and a mean of 0.53 kW if only PV systems 2–21 are considered. The RMSE range is from 0.66 kW to 2.51 kW with the PV1-based outlier of 8.29 kW and the overall average of 1.97 kW and 1.40 kW for PV2 to PV21, respectively. The CC is around 0.86 with the outlier of 0.74 for PV21 because of the large mismatch between the real and assumed orientation angles. The accumulated PV feed-in power on transformer level results in a ME of 10.46 kW and an RMSE of 21.33 kW, while the CC is 0.89.

The normalized ME ranges from 0.04 kW/kWp to 0.11 kW/kWp with a mean of 0.06 kW/kWp while the normalized RMSE ranges from 0.13 kW/kWp to 0.22 kW/kWp with a mean of 0.15 kW/kWp. Since the assumed orientation significantly increases the normalized ME (by 46% in this case), it is recommended to use real orientations in simulation studies.

4.5. Sensitivity to irradiance source

Ground measurements are point measurements and do not fully represent the spatial variability of a distributed PV fleet in an area. In addition ground measurement sites are sparse and it is unlikely that a ground observation exists within the area being simulated, as is also the case for this study. Therefore, we can quantify an example of such a representativeness error.

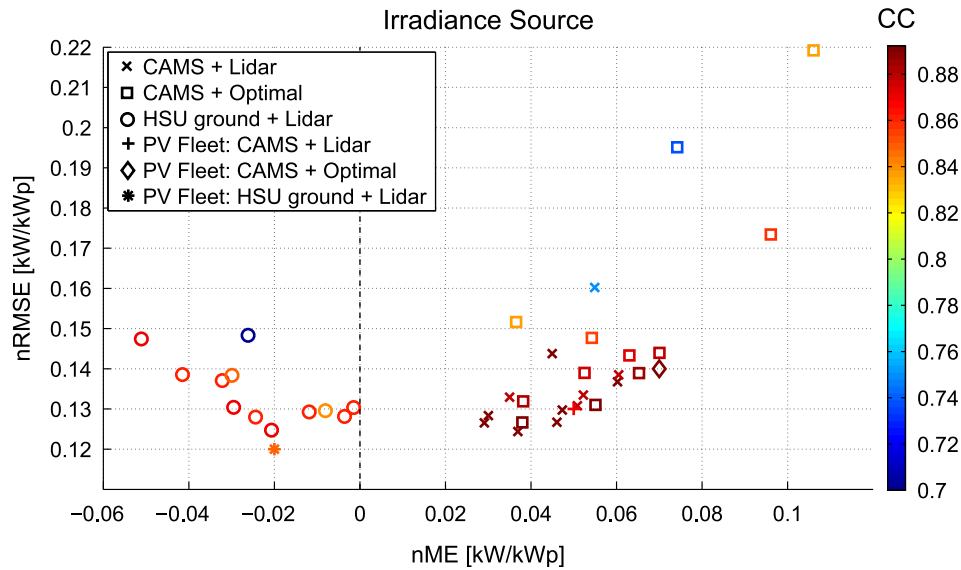


Fig. 6. Statistical values of PV feed-in power measurements based on Heliosat-4 derived irradiances and assumed optimal PV system orientation (rectangles) as well as ground-measured irradiances considering the real orientation (circles) against smart meter measurements. For comparison, the results of Table 2 are also shown. The markers express the normalized ME (nME, x-coordinate) and normalized RMSE (nRMSE, y-coordinate) as well as the color-coded CC. (For interpretation of the references to color in this figure legend, the reader is referred to the web version of this article.)

A simulation was performed using the measured irradiance data from the weather station for all PV systems. This is compared to results based on local satellite data. The BHI was estimated with the DIRINT method (Ineichen et al., 1992) from the ground-measured GHI. All other parameters were chosen as in Section 4.2. Fig. 6 shows the results of this simulation as circles. The ME ranges from -0.44 kW to -0.01 kW with an additional outlier of -1.25 kW at PV1. The averaged ME is -0.30 kW and -0.21 kW if only PV systems 2–21 are considered, respectively. The RMSE ranges from 0.61 kW to 2.2 kW with the PV1-based outlier of 7.1 kW and the overall average of 1.71 kW. If PV1 is excluded, the average RMSE is 1.23 kW. The CC is around 0.85 with the outlier of 0.70 for PV1. The accumulated PV feed-in power at transformer level results in a ME of -3.6 kW and an RMSE of 17.95 kW, while the CC is 0.85. The normalized ME ranges from -0.05 kW/kWp to 0 kW/kWp with a mean of -0.02 kW/kWp while the normalized RMSE ranges from 0.12 kW/kWp to 0.15 kW/kWp with a mean of 0.13 kW/kWp. The ME using ground-measured irradiances generally we found to be negative, while satellite-derived irradiances result in positive ME values. For nRMSEs the values we found to be comparable between satellite and ground-measured irradiances. The mean RMSE of the PV fleet excluding PV1 is slightly higher (0.8%) for the ground-measurements. It is assumed that this difference is caused by the distance to the test site. The positive bias of the satellite data (Section 4.1) can be seen clearly while the local measurement station provides an underestimation of nearly the same amount. As a positive ME is seen as an additional safety margin in our extended application of grid planning, in our case the satellite use is advantageous despite its slightly larger biases.

5. Validation of threshold exceedance monitoring

Up to now we used statistical measures as ME, RMSE or CC. Threshold exceedance monitoring as used for grid planning typically applies scores based on contingency tables (Wilks, 2011). These includes the measures called proportion correct (PC), contingency table bias (CTB), probability of detection (POD) and false alarm rate (FAR).

The worst possible PC is 0 and the best is 1. It shows the number correct simulations of events of interest related to the whole sample size. The CTB is the comparison of the average simulation to the average measurement. It is defined as the ratio of the number of simulated to the number of actually measured events. Simulations without any bias are $CTB = 1$. For $CTB < 1$ and $CTB > 1$ the events are under- and overestimated, respectively. The POD is defined as the fraction of interested events which are correctly calculated compared to all happen events. The range is between 0 and 1, while 1 is a perfect calculation. Furthermore, the FAR describes the number of false calculation results related to the number of simulated events. A perfect calculation is given for 0 while a complete mismatch results in 1. The results of these scores for the single PV systems and the lumped power of the PV fleet are presented in Table 3. The feed-in power of PV1 does not reach 70% of the rated PV power and leads to invalid scores.

The PC shows a high detection rate above 0.91 of the overstepping of the 70% PV feed-in power for all PV systems including PV1. The CTB for each system is larger than one meaning the detection is overestimated. This is a result of the overestimation found in CAMS Radiation Service irradiance. The POD shows values of at least 74% for single PV systems with an outlier for PV 1. The overall POD for

Table 3

Scores for overstepping 70% PV rated power feed-in power measurements based on Heliosat-4 derived irradiances against smart meter measurements.

PV system	PC	CTB	POD	FAR
PV1	0.94	36.98	0.14	1
PV2	0.93	1.26	0.75	0.4
PV8	0.93	1.75	0.83	0.52
PV10	0.91	2.54	0.84	0.67
PV13	0.93	1.31	0.77	0.41
PV14 + 15	0.93	1.25	0.83	0.33
PV16	0.91	2.74	0.82	0.7
PV17	0.92	2.23	0.84	0.62
PV18	0.93	1.36	0.76	0.44
PV19	0.93	1.17	0.74	0.37
PV20	0.91	2.78	0.82	0.71
PV21	0.94	1.81	0.8	0.56
PV fleet	0.93	3.89	0.66	0.83

the sum of the PV fleet is 66%. The FAR ranges from 0.33 to 0.71 and has a mean of 0.52 with an outlier of 1.00 for PV 1. Therefore, the possibility of PV feed-in power threshold detection should be considered with care as a systematic overestimation is found. However, this error will result in excessive grid reinforcement. At least, any planning based on this scheme will not compromise the grid security.

6. Application to power calculation at a transformer location

This section gives an example application of the proposed approach for DSOs. The active power at the transformer supplying the test site is calculated as a time series in 15-min resolution for a sample day. Besides the 12 PV systems used so far, the 9 additional PV systems installed at the test site are taken into account. The statistical measures of the 12 PV systems equipped with smart meters are determined in Section 4.1. A similar behavior is assumed for the other PV systems. Their PV feed-in power is calculated as well with the model described in Section 3 and added to the overall PV feed-in power.

The accumulated active power consumption of the 133 buildings is assumed as a standard load profile representing the state-of-the-art used by the DSOs in Germany (Fünfgeld and Tiedemann, 2000). The load profile is scaled to the annual energy consumption of each house provided by the DSO and aggregated to the test site's load curve. The resulting time series of the active power at the transformer can be computed by subtracting the PV feed-in power from the expected power consumption (Fig. 1).

It is planned to use the approach for a historic, multi-year dataset to quantify the need and benefit of grid enhancements and to define priorities on hardware replacement in the grid enforcement process. In preparation of this approach we provide the discussion of a single day. The result for 3rd August 2012 is shown in Fig. 7.

There is no deviation between measurement and calculation between 0:00 to 2:00 UTC and 21:00 to 24:00 UTC. In the morning hours after 2:00 UTC the calculated active power increases following the load profile while the measurement is almost constant at 50 kW. Obviously, the standard load profile deviates from the observations. This is a frequently found problem in grid planning but cannot be addressed within the scope of this paper. At approximately 7:00 UTC the difference between the assumed load profile and the simulation increases because of the increasing impact of

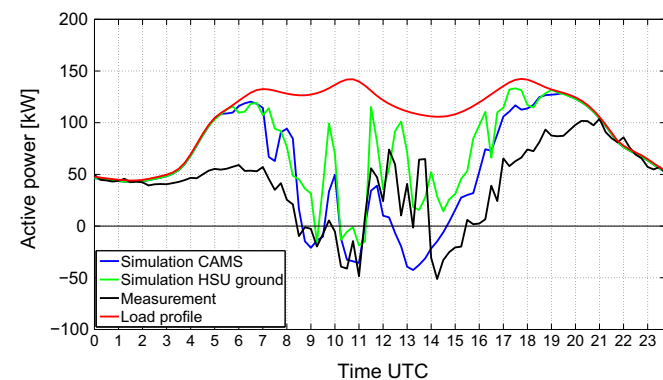


Fig. 7. Combination of simulated PV feed-in power and assumed standard load profile on 3rd August 2012 compared with measurements at the transformer. The blue line is the simulated active power at the transformer using CAMS Radiation Service, the green line is the simulation using the ground measured irradiance and the black line is the measurement. The red line indicates the assumed standard load profile for this day. (For interpretation of the references to color in this figure legend, the reader is referred to the web version of this article.)

the PV feed-in power. At the same time the measured active power decreases as well. The measurement and the calculation reach the zero line at around 8:30 UTC for the first time. The following negative active power values represent a so-called reverse load flow. The PV systems feed-in more power than consumed in the test site. The excess power is fed back to the medium voltage grid. This state changes several times during the day depending on the amount of solar irradiance. The PV feed-in power decreases again in the afternoon following the diurnal cycle. Nevertheless, the standard load profile remains too high. There is a difference between simulation and measurement probably because the true consumption is lower than assumed. The calculated active power and assumed load profile converge at around 19:30 UTC.

The combination of PV feed-in power and the standard load profile at the low voltage level shows a significant improvement compared to the case of the standard load profile neglecting the PV feed-in power. The overall trends including the reversal load flows are correctly simulated. The change from reversal load flow to regular load flow around 12:00 UTC is detected, however, the amplitude and duration varies. The simulation provides a realistic time series for the case study considering the PV feed-in power and consumption. Even if not all values are exactly simulated, this is helpful for an economic grid planning and operation by the DSO as well as for impact studies of new mitigation measures.

7. Conclusion and outlook

The usefulness of satellite-derived irradiance data from CAMS Radiation Service for the PV feed-in power calculation of residential PV systems in a small-scale distribution grid is investigated.

The PV model uses the nominal PV power, the location and the orientation angles as site-specific input parameters. As the orientation angles are normally not available from the DSO, they have to be provided by external data sources as e.g. airborne laser-scan data as done in this study. Using only a standard orientation (30° inclination versus south) instead of the actual orientation is not recommended. The errors increase by 46% for the overall ME and by 13% for the overall RMSE in our test case. On the other hand, the selection of the PV module technology has no significant impact. The smart meters used in this work were installed during a research measurement campaign by the DSO. It is assumed, that the orientation of the PV systems can also be estimated by measured feed-in power time series. However, the recent draft of the law for digitization of the energy transition in Germany stipulates the installation for smart meters only for PV systems larger than 7 kWp. Additionally, an installation of smart meters in all residential PV systems will take time and is not expected to be available soon.

If using irradiance ground measurements from the nearest available meteorological station 11 km away, an increase by 0.8% is found for the RMSE. The RMSE is similar for both satellite-derived and ground-measured irradiances but slightly higher for the ground-measured data. The validation of the satellite GHI with ground measurements shows similar positive biases as observed previously in the literature. Therefore, the ME is positive for all PV system if satellite data are used. It is found to be negative if ground-measured data are used, but the absolute values are comparable. The overestimation of satellite irradiance data is more acceptable as they provide an additional safety margin in grid planning while underestimations as found for the ground observation may provide a false sense of grid security. This is to be avoided under any circumstances. Nevertheless, satellite biases should be reduced for an economically optimal decision.

The calculated PV feed-in power is compared with smart meter measurements and shows almost constant normalized ME and

RMSE for all PV systems. Therefore, it can be assumed that the errors are independent of the nominal power and for small and large PV systems as used in residential areas.

Scores on the detection accuracy of whether the specific PV system reaches a defined feed-in power threshold are applied. However, further reduction in satellite biases are necessary to increase the detection accuracy.

Overall, it is appropriate to apply satellite-based irradiance data for residential PV systems. This allows the simulation of each single PV system in larger PV fleets as found nowadays in low voltage grids. The use of ground-based irradiance measurements is neither required nor recommended in our case. The economic comparison of GHI ground measurements at the transformer site for PV feed-in power simulation versus satellite-based methods will be part of future investigations. It has to be noted that in the field of PV system monitoring, the large number of GHI measurement devices turned out to be difficult to handle in practice and causes non-negligible maintenance and controlling costs while the satellite is a single instrument where maintenance and ground segment is already performed by the satellite agency paid from taxpayers. Therefore, a detailed and complete cost assessment is recommended.

Local shadowing effects are not considered in this study but it is assumed that these will increase the accuracy of the simulation model. There are several approaches in literature to realize a shadowing time-series (e.g. Jakubiec and Reinhart, 2013; Borfecchia et al., 2014; Fath et al., 2015).

The approach introduced can be extended to load flow calculations by using detailed load information. An example is given for the calculation of the active power at the test site transformer and compared with measurements. It illustrates the value and need of introducing PV feed-in in grid simulations as standard load profiles do not take this into account. Further research and analysis is ongoing in order to improve this application, and to especially deal with the imperfect load profile if applying existing standard load profiles on the transformer level.

DSOs have to maintain voltage variations in the distribution grid within bounds. Therefore, they need information on both voltage values and voltage drops. We demonstrated an approach to calculate load flow affecting the voltage values for certain times and locations with high numbers of PV systems. In future, the PV feed-in power calculation based on satellite irradiance data can be combined with grid simulation tools.

These methods will support DSOs in the strategic planning of their infrastructure re-enforcement in areas with already or expected increases in PV shares. Based on multi-year historic irradiance databases starting in 2004 it will also allow simulating larger PV shares being expected in the future, based on realistic both spatially and temporally resolved input data. Additionally, the use of near-real time satellite information will allow DSOs the monitoring of their assets in near real-time. Moreover, these methods can be applied for predicted irradiance data from either cloud-motion-vectors from satellite scenes or numerical weather model forecasts for short-term predictions in daily grid operations.

Acknowledgments

The research leading to these results has received funding from the European Union's Seventh Framework Programme (FP7/2007–2013) under grant agreement No. 262892 (project ENDORSE) and No. 608930 (project OrPHEuS), as well as from the German Federal Ministry of Education and Research under support code 03FH03013 (project NATHAN-PV).

The authors would like to thank Florian Meier at Stadtwerke Ulm/Neu-Ulm Netze GmbH for providing the smart meter measurements, the annual energy consumption of the test site and

electric grid-related data as well as discussions about the DSO interests.

References

- Agricola, A.-C., Seidl, H., Mischinger, S., Rehtanz, C., Greve, M., Häger, U., Hilbrich, D., Kippelt, S., Kubis, A., Liebenau, V., Noll, T., Rüberg, S., Schlüter, T., Schwippe, J., Spieker, C., Teuwsen, J., 2014. Systemdienstleistungen 2030: Sicherheit und Zuverlässigkeit einer Stromversorgung mit hohem Anteil erneuerbarer Energien.
- Albrecht, W., Schröder, W., 2013. Ausführungshandbuch für Photovoltaik-Anlagen: Normgerechte Planung, Montage, Installation, Inbetriebnahme und Wartung, stand märz 2013 ed. Forum, Merching.
- Bendib, B., Belmili, H., Krim, F., 2015. A survey of the most used MPPT methods: conventional and advanced algorithms applied for photovoltaic systems. *Renew. Sust. Energy Rev.* 45, 637–648.
- Beyer, H.G., Betcke, J., Drews, A., Heinemann, D., Lorenz, E., Heilscher, G., Bofinger, S., 2004. Identification of a general model for the MPP performance of PV-modules for the application in a procedure for the performance check of grid connected systems. In: Hoffmann, W. (Ed.), Nineteenth European Photovoltaic Solar Energy Conference. WIP-Renewable Energies and ETA, pp. 3073–3076.
- Beyer, H.G., Martinez, J.P., Suri, M., Torres, J.L., Lorenz, E., Müller, S., Hoyer-Klick, C., Ineichen, P., 2009. Report on Benchmarking of Radiation Products: Deliverable 1.1.3.
- Borfecchia, F., Caiaffa, E., Pollino, M., Cecco, L.D., Martini, S., La Porta, L., Marucci, A., 2014. Remote Sensing and GIS in planning photovoltaic potential of urban areas. *Eur. J. Remote Sens.*, 195–216.
- Bucher, C., Betcke, J., Andersson, G., Bletterie, B., Küng, L., 2012. Simulation of distribution grids with photovoltaics by means of stochastic load profiles and irradiance data. In: Nowak, S., Jäger-Waldau, A., Helm, P. (Eds.), 27th European Photovoltaic Solar Energy Conference. WIP, München, pp. 3795–3800.
- DGS, 2015. EEG Plant Register: 03/2015. <www.energymap.info/download.html> (accessed 24.04.15).
- DIN EN 50470-3, 2007. Electricity Metering Equipment (a.c.) – Part 3: Particular Requirements – Static Meters for Active Energy (Class Indexes A, B and C).
- EEG, 2014. Renewable Energy Law (German): Gesetz für den Ausbau erneuerbarer Energien (Erneuerbare-Energien-Gesetz – EEG 2014).
- EnWG, 2013. Law on the Energy Industry. *Energiewirtschaftsgesetz, German*.
- Fath, K., Stengel, J., Sprenger, W., Wilson, H.R., Schultmann, F., Kuhn, T.E., 2015. A method for predicting the economic potential of (building-integrated) photovoltaics in urban areas based on hourly radiance simulations. *Sol. Energy* 116, 357–370.
- Fünfgeld, C., Tiedemann, R., 2000. Anwendung der Repräsentativen VDEW-Lastprofile: Step-by-step.
- Glunz, S.W., Preu, R., Biro, D., 2012. Crystalline silicon solar cells. In: Sayigh, A. (Ed.), *Comprehensive Renewable Energy*. Elsevier, pp. 353–387.
- Grossi, L., Wirth, G., Lorenz, E., Spring, A., Becker, G., 2014. Simulation of the feed-in power of distributed PV systems. In: 29th European PV Solar Energy Conference and Exhibition. WIP, pp. 2916–2920.
- Hoff, T.E., Perez, R., 2012. Modeling PV fleet output variability. *Sol. Energy* 86 (8), 2177–2189.
- Ineichen, P., Perez, R.R., Seal, R.D., Maxwell, E.L., Zalenka, A., 1992. Dynamic global-to-direct irradiance conversion models. *ASHRAE Trans.* 98 (1), 354–369.
- ISO 9060, 1990. Solar Energy – Specification and Classification of Instruments for Measuring Hemispherical Solar and Direct Solar Radiation.
- Jakubiec, J.A., Reinhart, C.F., 2013. A method for predicting city-wide electricity gains from photovoltaic panels based on LiDAR and GIS data combined with hourly Daysim simulations. *Sol. Energy* 93, 127–143.
- Katzmaier, M., 2015. Personal Communication with Martin Katzmaier, Team Leader Measurement Electric Power at Stadtwerke Ulm/Neu-Ulm Netze GmbH, 7.4.2015.
- King, D.L., Boyson, W.E., Kratochvill, J.A., 2004. Photovoltaic Array Performance Model. Albuquerque, USA. <prod.sandia.gov/techlib/access-control.cgi/2004/043535.pdf> (accessed 01.03.15).
- King, D.L., Gonzalez, S., Galbraith, G.M., Boyson, W.E., 2007. Performance Model for Grid-Connected Photovoltaic Inverters. Albuquerque, USA. <prod.sandia.gov/techlib/access-control.cgi/2007/075036.pdf> (accessed 22.02.15).
- Krauter, S., Grunow, P., Preiss, A., Rindert, S., Ferretti, N., 2008. Inaccuracies of input data relevant for PV yield prediction. In: 2008 33rd IEEE Photovoltaic Specialists Conference (PVSC), pp. 1–5.
- Kühnert, J., Lorenz, E., Betcke, J., Hammer, A., Heinemann, D., 2014. Regionale PV-Leistungsvorhersagen für den Kurzzeit-Bereich auf Basis von Satellitendaten, numerischen Wetterprognosen und PV-Leistungsmessungen. In: OTTI (Ed.), 29. Symposium Photovoltaische Solarenergie. 12. bis 14. März 2014, Kloster Banz, Bad Staffelstein.
- Lave, M., Kleissl, J., Stein, J.S., 2013. A wavelet-based variability model (WVM) for solar PV power plants. *IEEE Trans. Sust. Energy* 4 (2), 501–509.
- Lefèvre, M., Oumbe, A., Blanc, P., Espinar, B., Gschwind, B., Qu, Z., Wald, L., Schroedter-Homscheidt, M., Hoyer-Klick, C., Arola, A., Benedetti, A., Kaiser, J.W., Morcrette, J.-J., 2013. McClear: a new model estimating downwelling solar radiation at ground level in clear-sky conditions. *Atmos. Meas. Tech.* 6 (9), 2403–2418.
- Leloux, J., Narvarte, L., Trebosc, D., 2012a. Review of the performance of residential PV systems in Belgium. *Renew. Sust. Energy Rev.* 16 (1), 178–184.

- Leloux, J., Narvarte, L., Trebosc, D., 2012b. Review of the performance of residential PV systems in France. *Renew. Sust. Energy Rev.* 16 (2), 1369–1376.
- Loutzenhiser, P., Manz, H., Felsmann, C., Strachan, P., Frank, T., Maxwell, G., 2007. Empirical validation of models to compute solar irradiance on inclined surfaces for building energy simulation. *Sol. Energy* 81 (2), 254–267.
- Meier, F., 2014. Personal Communication with Florian Meier, Head of Grid Planning, Stadtwerke Ulm/Neu-Ulm Netze GmbH, 21.10.2014.
- Meteotest, 2015. Homepage meteonorm. <<http://meteonorm.com/>> (accessed 09.10.15).
- NAV, 2006. Niederspannungsanschlussverordnung: NAV.
- Nguyen, A., Velay, M., Schoene, J., Zheglov, V., Kurtz, B., Murray, K., Torre, B., Kleissl, J., 2016. High PV penetration impacts on five local distribution networks using high resolution solar resource assessment with sky imager and quasi-steady state distribution system simulations. *Sol. Energy* 132, 221–235.
- Oumbe, A., Qu, Z., Blanc, P., Lefèvre, M., Wald, L., Cros, S., 2014. Decoupling the effects of clear atmosphere and clouds to simplify calculations of the broadband solar irradiance at ground level. *Geosci. Model Develop.* 7 (4), 1661–1669.
- Pardatscher, R., Witzmann, R., Wirth, G., Becker, G., Garhamer, M., Brantl, J., 2011. Untersuchung zu den Auswirkungen von Photovoltaikeinspeisung auf das Nieder- und Mittelspannungsnetz. In: *Internationaler ETG-Kongress 2011*. VDE-Verlag.
- Qu, Z., Oumbe, A., Blanc, P., Espinar, B., Gesell, G., Gschwind, B., Klüser, L., Lefevre, M., Saboret, L., Schroedter-Homscheidt, M., Wald, L., 2016. Fast radiative transfer parameterisation for assessing the surface solar irradiance: the heliosat-4 method. *Meteorol. Z.* (in press).
- Reindl, D., Beckman, W., Duffie, J., 1990a. Diffuse fraction correlations. *Sol. Energy* 45 (1), 1–7.
- Reindl, D., Beckman, W., Duffie, J., 1990b. Evaluation of hourly tilted surface radiation models. *Sol. Energy* 45 (1), 9–17.
- Renné, D., 2014. Emerging meteorological requirements to support high penetrations of variable renewable energy sources: solar energy. In: Troccoli, A., Dubus, L., Haupt, S.E. (Eds.), *Weather Matters for Energy*. Springer, New York, pp. 257–273.
- Rikos, E., Tselepis, S., Hoyer-Klick, C., Schroedter-Homscheidt, M., 2008. Stability and power quality issues in microgrids under weather disturbances. *IEEE J. Sel. Top. Appl. Earth Observ. Remote Sens.* 1 (3), 170–179.
- Ruf, H., Funk, D., Meier, F., Heilscher, G., 2015. Bestimmung von Ausrichtungs- und Neigungswinkeln von Bestandsanlagen mittels LIDAR Daten. In: OTTI (Ed.), 30. Symposium Photovoltaische Solarenergie. 4. bis 6. März 2015, Kloster Banz, Bad Staffelstein.
- Stein, J., Perez, R., Parkins, A., 2010. Validation of PV performance models using satellite-based irradiance measurements: a case study. In: Campbell-Howe, R. (Ed.), 39th ASES National Solar Conference. American Solar Energy Society.
- Stein, J.S., 2012. The photovoltaic performance modeling collaborative (PVP/MC). In: 38th IEEE Photovoltaic Specialists Conference (PVSC). IEEE, pp. 003048–003052.
- TAB, 2009. Technische Anschlussbedingungen für den Anschluss an das Niederspannungsnetz: TAB 2007: mit BDEW-Ergänzungen. Berlin.
- Ueda, Y., Kurokawa, K., Kitamura, K., Yokota, M., Akanuma, K., Sugihara, H., 2009. Performance analysis of various system configurations on grid-connected residential PV systems. *Sol. Energy Mater. Sol. Cells* 93 (6–7), 945–949.
- Verso, A., Martin, A., Amador, J., Dominguez, J., 2015. GIS-based method to evaluate the photovoltaic potential in the urban environments: the particular case of Miraflores de la Sierra. *Sol. Energy* 117, 236–245.
- Wilks, D.S. (Ed.), 2011. *International Geophysics: Statistical Methods in the Atmospheric Sciences*. Academic Press.
- Wirth, G., Spring, A., Becker, G., Pardatscher, R., Ldl, M., Witzmann, R., Brantl, J., Garhamer, M., Wagenhuser, H., 2011. Felduntersuchung der Netzauslastung und Spannungsanhebung durch PV-Anlagen. In: Strauß, P. (Ed.), 26. Symposium Photovoltaische Solarenergie. OTTI.
- WMO, 2008. Guide to meteorological instruments and methods of observation, WMO, seventh ed., Vol. 8. World Meteorological Organization, Geneva, Switzerland <<https://www.wmo.int/pages/prog/www/IMOP/CIMO-Guide.html>>.
- Zarzalejo, L.F., Polo, J., Martín, L., Ramírez, L., Espinar, B., 2009. A new statistical approach for deriving global solar radiation from satellite images. *Sol. Energy* 83 (4), 480–484.